ELSEVIER

Contents lists available at ScienceDirect

# Earth and Planetary Science Letters

www.elsevier.com/locate/epsl



# The Northern Gulf Anomaly: P- and S-wave travel time delays illuminate a strong thermal feature beneath the Northern Gulf of Mexico



Zoe Krauss\*, William Menke

Lamont-Doherty Earth Observatory, 61 Rte 9W, Palisades, NY, 10964, USA

#### ARTICLE INFO

# Article history: Received 12 August 2019 Received in revised form 11 January 2020 Accepted 15 January 2020 Available online xxxx Editor: M. Ishii

Keywords:
EarthScope Transportable Array
USArray
edge-driven convection
asthenospheric upwelling
Gulf of Mexico

#### ABSTRACT

Seismic measurements are used in a detailed investigation of a region of extremely low asthenospheric seismic velocities along the US Gulf Coast, first imaged in continental-scale geotomography, which we term the Northern Gulf Anomaly (NGA). Differential P- and S-wave arrival times from teleseisms at a variety of back-azimuths, observed on EarthScope Transportable Array stations near the US Gulf Coast, demonstrate that asthenospheric seismic velocities are 8-10% lower than the neighboring craton, and define the spatial extent and character of the anomaly. Travel time anomalies are calculated relative to the AK135 earth model and corrected to account for the effect of the kilometers-thick sedimentary cover in the region. The NGA is most intense at the southernmost coast of Louisiana and East Texas (with an eastern edge at 89°W) and smoothly tapers away in a triangular wedge that extends inland as far as 300 km. It has sharper edges and a smaller areal extent (by  $\sim$ 50%) than previously-published geotomography has indicated. Both the magnitude and ratio of delays indicate that the NGA has a thermal origin, which may represent past or present-day small-scale convective upwelling near the southeastern edge of the North American continent. The NGA suggests that large-scale but poorly understood asthenospheric processes are at work beneath the US Gulf Coast, notwithstanding this region's reputation as an aseismic, passively-subsiding continental margin.

© 2020 Elsevier B.V. All rights reserved.

#### 1. Introduction

Deployment of the continental-scale Earthscope Transportable Array (TA) has led to the recent publication of highly detailed geotomographic maps of the conterminous Unites States (e.g. Schmandt and Lin, 2014; Shen and Ritzwoller, 2016; Golos et al., 2018; Porter et al., 2016). These studies bring to light several previously unimaged slow-seismic-velocity anomalies, possibly caused by asthenospheric upwelling (e.g. Menke et al., 2016; Byrnes et al., 2019). Imaged in these recent maps is a significant anomaly on the northern coast of the Gulf of Mexico, centered in northern Louisiana and extending northward, with significantly low shear velocities extending to about 400 km depth, which we refer to as the Northern Gulf Anomaly (NGA). An anomaly of this strength is normally associated with volcanism, faulting, seismicity, uplifting, etc., but these processes are either not currently active, or occur at

relatively low rates, in the area of the NGA. This study is the first focused investigation into the characteristics and potential origin of the NGA, using high-quality teleseismic body wave travel time anomalies to clearly define its magnitude and extent.

#### 1.1. Tectonic setting

The most recent large-scale tectonic event to occur in the area of the NGA was the opening of the Gulf of Mexico, as the Yucatan block split from the North American plate (Bird et al., 2005; Pilger, 1981). The opening began with continental extension between 160 and 150 Ma, with an initial 22° counterclockwise rotation of the Yucatan block away from North America. Seafloor spreading occurred between 150 and 140 Ma, creating another 20° counterclockwise rotation of the Yucatan block. It is believed that this rotation was accomplished by a single, now-extinct ocean-continent transform boundary (Bird et al., 2005). Due to deep burial beneath sediments, it is difficult to study the traces left by this tectonism. However, salt diapirs have exhumed samples indicating that the Texas coast consists of a magma-rich volcanic rifted margin, with the Louisiana coast representing a more magma-poor rifted passive margin (Mickus et al., 2009; Stern et al., 2011). The Sabine Uplift

<sup>\*</sup> Corresponding author. Present address: Department of Oceanography, University of Washington, 1501 NE Boat St, Seattle, WA, 98195, USA.

 $<sup>\</sup>hbox{\it E-mail addresses:} \ zkrauss@uw.edu \ (Z. \ Krauss), \ menke@ldeo.columbia.edu \ (W. \ Menke).$ 

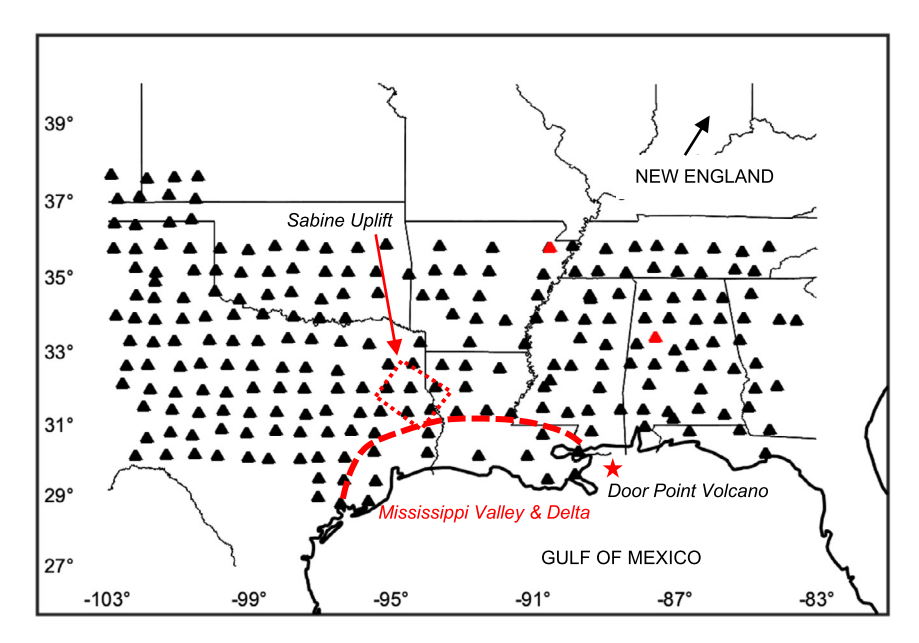


**Fig. 1.** Map of the study area for the NGA, displaying the 234 stations used to calculate differential travel times (black triangles). Only stations with available, clean data for chosen teleseisms were used, which differed with each teleseismic source group. The stations whose seismograms are shown in Fig. 3 are marked as red triangles: V43A is the more northern station, and Z48A is the station further south. The Mississippi Valley and Delta region, drawn to reflect the area of thickest sediment where 5 s Rayleigh waves are slowed by >48%, (Ekstrom, 2017), is outlined with a red dashed line. To give context of the location of the most recent local tectonic events, the Sabine Uplift (Adams, 2009) is outlined with a red dotted line, and the Door Point Volcano (Braunstein and McMichael, 1976) is marked with a red star. (For interpretation of the colors in the figure(s), the reader is referred to the web version of this article.)

(Fig. 1), marked by a magnetic high, was also created during the late Jurassic, bounded by northeast and southwest transform fault systems that ran parallel to the opening tectonics of the Gulf of Mexico (Adams, 2009). Some late Cretaceous (90 – 74 Ma) volcanism has been identified in Mississippi and Louisiana, including the Door Point Volcano (Fig. 1) (Braunstein and McMichael, 1976), but no Tertiary volcanism, uplift, or active tectonics have been identified along the Gulf Coast.

# 1.2. Ongoing local processes

The Mississippi Delta region in southern Louisiana, in the center of our study area, is an area of rapid on-going sedimentation, with deposits exceeding 110 km<sup>3</sup> in volume (Fisk et al., 1954). These low seismic velocity sediments are associated with some of the lowest short-period Rayleigh wave velocities in the US. Phase velocities, at 5 s period, are as much as 64% below the continental mean (Ekstrom, 2014, 2017) in the Mississippi Delta and Valley area (Fig. 1). Although the sediments and the NGA are not directly related, they occur in more-or-less the same geographical region and are both characterized by extremely-low seismic velocities. Their effect on seismic measurements must be quantified and removed from delay calculations in order to accurately assess the delay caused solely by the deeper asthenospheric anomaly.

Geodetic motions have been observed within parts of the study region, and especially around the Mississippi Delta, with subsidence rates up to 5 mm/yr, together with southward displacements of up to 2 mm/yr (Dokka et al., 2006). The cause of this subsidence is debated (Tornqvist et al., 2008; Wolstencroft et al., 2014), and variously ascribed to tectonic mechanisms, sediment loading, or other causes. Uplift would be expected during the emplacement of a large-scale mantle hotspot; the opposite is occurring here.

The seismicity rate in the study area is lower than much of the rest of the US. For instance, the US Geological Survey's ComCat database lists 117 earthquakes of magnitude  $\geq 3$  in the 1999-2019 time period for a  $15^{\circ} \times 8^{\circ}$  rectangle centered on the study area, whereas rectangles of the same size centered in New England and

central United States experienced 163 and 3203 earthquakes, respectively. Relatively large earthquakes (up to magnitude 5.8) have occurred; however, at least some of them are thought to be due to sediment slumping within the Gulf, and not to tectonism (Nettles, 2007).

#### 1.3. Analogous studies

The TA has revealed other low velocity anomalies in the asthenosphere along the eastern, passive margin of the North American continent. They include the Northern Appalachian Anomaly (NAA) in southern New England (Menke et al., 2016; Dong and Menke, 2017; Levin et al., 2017) and the Central Appalachian Anomaly (CAA) near the Virginia - West Virginia border (Byrnes et al., 2019). Geotomography indicates that the NAA is an intense anomaly centered at about 200 km depth in the asthenosphere with a maximum shear velocity contrast of about 8% (Menke et al., 2016). Low compressional-to-shear wave velocity ratios (Menke et al., 2016) and high seismic attenuation (Dong and Menke, 2017) indicate that the anomaly is thermal (as opposed to compositional) in origin. High seismic attenuation at the CAA indicate that it has a thermal origin as well (Byrnes et al., 2019). Both of these anomalies may represent edge-driven convection cells (King and Anderson, 1998) along the passive margin that are associated with lithospheric delamination (Menke et al., 2016, 2018; Byrnes et al., 2019). Unusually low shear wave splitting suggests vertical flow beneath the NAA, and the overall lack of obvious surface trace or uplift in the area lead Levin et al. (2017) to infer that the upwelling is recently formed. A key issue is whether the NGA is another example of this style of lithospheric upwelling - or something else, entirely.

We examine the NGA using a simple approach of body wave travel time delays. Recent TA-based geotomographic images of the North American continent utilized both body and surface wave data, but are highly reliant on the teleseismic body wave travel time delay data to image structures deeper than  $\sim\!150$  km. Teleseismic body wave data from the TA has very dense spatial coverage, due to small (75 km) interstation distances, but very poor

angular coverage, since only a few large teleseismic earthquakes occur during the short (2 yr) deployment period of each of the TA's stations. Geotomography works best when angular coverage is complete; otherwise depth resolution is poor (e.g. Menke, 2005). Furthermore, the less complete the angular coverage, the more regularization (smoothing) is needed to stabilize the inversion and regularization tends to smooth the edges of anomalies, reduce their overall amplitude and (in the worst case) lead to the appearance of artifacts in the images. Our approach here is to focus on delay times from just a few very high-quality teleseisms. We interpret both the delay time maps for individual teleseisms (which have high horizontal resolution) and a coarse tomographic inversion of the entire dataset (which provides some depth control). As we will demonstrate below, the delay time maps alone are sufficient to establish the NGA is a thermal anomaly that extends throughout the entire asthenosphere. The tomography supports these inferences, which are very robust.

# 1.4. Importance of investigation

An in-depth investigation of the NGA begins to shed light on the unknown tectonic mechanism that creates visibly inactive hotspots. As the NGA had been unimaged until the unprecedented coverage of the TA, it is possible these types of features are ubiquitous on the earth, but remain undetected. Identifying this mechanism will aid in the understanding of tectonic histories elsewhere on the planet.

Recognition of the NGA as an intense thermal anomaly would significantly change the narrative of the geologic history of the Gulf of Mexico. The presence of an active asthenospheric upwelling would likely have an effect on the current geotherm, perhaps influencing oil maturation and salt migration, both of which are important factors to those who rely on the resources within the Gulf. Additionally, the presence of a large source of heat in the mantle has the potential to cause future volcanic or seismic hazard. Fundamental characterization of this anomaly is therefore essential to not only the complete understanding of the anomaly's effects on both local geologic processes and larger-scale societal welfare, but also a thorough understanding of asthenospheric-lithospheric interactions in general.

#### 2. Methodology

# 2.1. Calculation of travel times

Using source parameters from the US Geological Survey's Com-Cat database, ten earthquakes were selected (Fig. 2, Table 1) with moment magnitudes  $M_w \ge 6$  so as to ensure clear signals that would appear above noise on the maximum amount of stations. Epicentral distances from the NGA between 30° and 80° were chosen to minimize ray interactions with both near-surface and mantle features. Broadband seismic time series, instrument responses and other metadata for 234 Transportable Array (TA) stations (Fig. 1) were downloaded from the Incorporated Research Institutions for Seismology's (IRIS's) Data management system. TA stations were deployed, decommissioned and re-deployed in twoyear cycles, moving progressively eastward across the study area, which is larger than any concurrently-operated group of stations. To resolve this issue, we constructed a virtual array that spanned the study area by combining earthquakes with similar locations. These "source groups" were defined as follows: Aleutian Trench; Cascadia margin; Central America; and Nazca margin (Fig. 2, Ta-

Seismograms were interpolated to a common time base and 0.01~s sampling interval, converted to displacement by deconvolution of the instrument response, and band-pass filtered using a

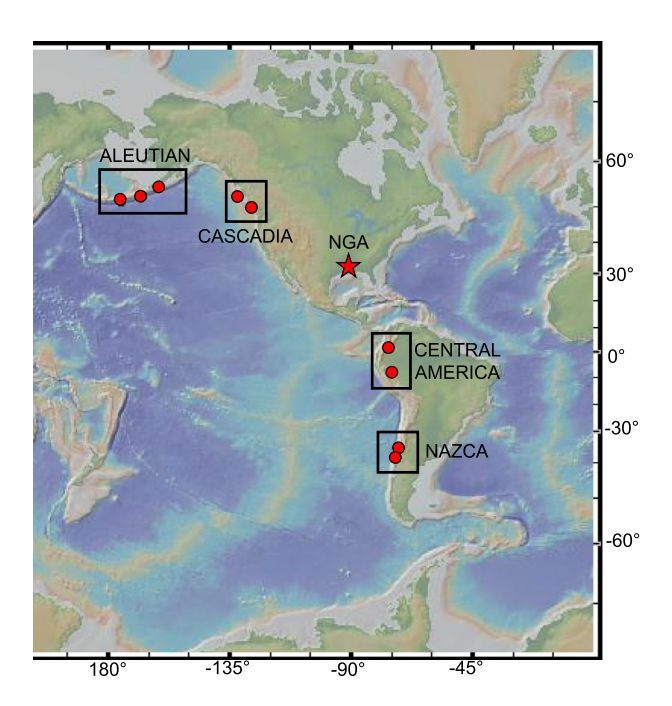


**Fig. 2.** Map with locations of all teleseismic earthquakes (red circles) used in this study of the NGA, with teleseisms organized into their source groups (black boxes). The generalized location of the NGA is marked with a red star. Figure made using GeoMapApp (www.geomapapp.org) (Ryan et al., 2009).

Chebyshev filter between 0.01 and 0.03 Hz. The streams were subsequently rotated into vertical, radial and transverse components. Predicted P- and S-wave arrival times were calculated using the AK135 earth model (Kennett et al., 1995). All seismograms were vetted by plotting, overlaying them with predicted arrival times, visually assessing quality and discarding those with malfunctioning components, high noise levels, etc. Differential arrival times between pairs of stations recording a common earthquake were calculated by cross-correlation, after windowing and tapering the seismograms around the predicted arrival times. P- and S-wave differential times were estimated from the vertical and radial component, respectively. The peak value of the cross-correlation was used to assess the quality of each differential time measurement. The event-mean cross-correlation values ranged between 0.90 and 0.98. An example of how this cross-correlation technique is used to calculate differential travel time can be found in Fig. 3.

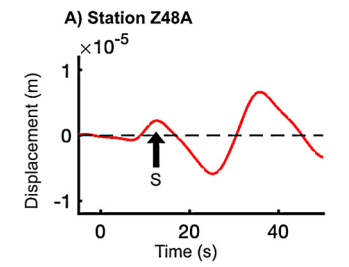
#### 2.2. Correlation of source groups

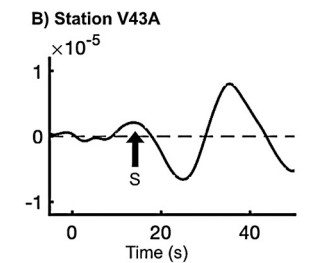
Although we assign a "travel time" to each station that observes a given earthquake, only time differences between stations are meaningful; an arbitrary time offset can be added to the travel times of all stations observing a common earthquake without affecting the differential times. This ambiguity arises since of the measurement technique is based on the determination of time offsets using cross-correlation. However, it also reflects a broader issue encountered in this and other regional studies. Source-side velocity heterogeneities, which affect all the waves observed in the study region more-or-less uniformly, are difficult to model and, in this analysis, treated as an unknown.

Although a given earthquake was observed on only a subset of stations in the virtual array due to their short deployment cycles, overlap occurred in which some stations observed two or more earthquakes from a given source group. Consequently, a time offset for each earthquake can be applied to match up the travel times of the overlapping stations. Although these adjustments change the "zero level" of the travel times, the magnitude of relative delays

**Table 1**Characteristics of teleseisms used for this study of the NGA, organized into their source groups. Offsets used to manually correlate the velocity perturbations between teleseisms in a given group can be found in the final two columns.

Source group	EQ location	EQ magnitude (Mw)	EQ date	EQ LAT	EQ LON	dT <sub>P</sub> offset (s)	dT <sub>S</sub> offset (s)	Depth (km)
Central America	Ecuador	7.1	2010/08/12	-1.266	-77.306	-0.1	1	206.7
	Northern Peru	7	2011/08/24	-7.641	-74.525	0	0	147
	Colombia	7.3	2012/09/30	1.929	-76.362	-0.4	-0.75	170
Aleutian Trench	Andreanof Islands	6.4	2010/10/08	51.374	-175.361	0	0.6	19
	Alaska Peninsula	6.1	2011/07/16	54.787	-161.29	0.2	0	36
	Fox Islands	6.2	2012/08/10	52.633	-167.421	0	-0.5	13
Cascadia margin	Vancouver Island	6.4	2011/09/09	49.535	-126.893	-0.1	0	22
	Haida Gwaii	6.2	2012/10/30	52.365	-131.902	0	-0.8	9
Nazca Trench	Araucania, Chile	7.2	2011/01/02	-38.355	-73.326	0	2	24
	Maule, Chile	7.1	2012/03/25	-35.2	-72.217	0	0	40.7





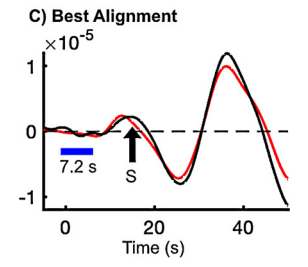


**Fig. 3.** Example of using cross-correlation to calculate the time difference of the S-wave arrivals on two stations observing the same event. (a) S-wave observed on the filtered radial-component of station Z48A (see Fig. 2 for location). (b) Identically-processed first S-wave arrival on station V43A (see Fig. 2 for location) from the same teleseism. (c) Best alignment using the cross-correlation method. Note the very similar appearance of the S-wave on the two stations and the qualitatively good alignment (maximum cross-correlation is 0.97). The NGA's 7.2 s peak-to-peak differential travel time anomaly is shown in blue, illustrating that any errors in alignment will be very small in comparison.

in preserved. The mismatch between travel times at the overlapping stations was typically less than 1 s (compared to a maximum anomaly of about 10 s). The values of the offsets applied to each earthquake event in order to correlate source groups can be found in Table 1.

# 2.3. Correction for sediment and crustal thickness

The Gulf Coast, and especially the Mississippi Valley (Fig. 1), contains thick deposits of low-velocity sediments that cause significant travel time delays. Their effect must be removed from the data in order to isolate the signal from mantle heterogeneities. Rayleigh waves are an effective proxy for the extent of sediment slowing effects, as they are strongly affected by near-surface slowing features. The areal distribution of the sediments is welldetermined by Ekstrom's (2017) delay maps of five second period Rayleigh wave phase velocity  $v_R$ . Utilizing this effect, we develop a method for estimating the P- and S-wave travel time  $(T_P \text{ and } T_S, \text{ respectively})$  associated with sediments in a region using Rayleigh wave phase velocity  $v_R$  as a proxy. First, we develop a simple crustal model with upper crustal thickness, fixed upper crustal (loose sediment) density of 2.0 g/cm<sup>3</sup>, and variable shear wave velocity  $v_S$  (with  $v_P = \sqrt{3}v_S$ ). Numerical tests indicate that, as expected, teleseismic travel time and Rayleigh wave phase velocity are mostly sensitive to vertical averages of uppercrustal properties. Consequently, we fix upper crustal thickness at 8 km, thick enough to encompass low-velocity sediments. Second. we use forward modeling to predict the Rayleigh wave velocity  $v_R(v_S)$  through the crustal model and the associated body wave travel times  $T_P(v_S)$  and  $T_S(v_S)$ . Third, we varied  $v_S$  to build up sets of  $(T_P, v_R)$  and  $(T_S, v_R)$  data. Fourth, we used least-squares to fit a cubic curve to these data, obtaining smooth functions  $T_P(v_R)$ and  $T_S(v_R)$ , which effectively capture the relationship between body wave velocities and Rayleigh wave velocities. With this relationship, we were able to use Ekstrom's (2017) gridded  $v_R$  data, which represents the effect of sediments on seismic velocities, to calculate the effect of sediments on our body wave travel times. We evaluated the smoothing functions for each station, using an estimate of  $v_R$  obtained with a two-dimensional interpolation of Ekstrom's (2017) gridded  $v_R$  data onto the station location, and applied the correction to the differential travel time anomaly data.

Crustal thickness variations also lead to travel time anomalies that can be as large as  $\sim 1$  s for S-waves, with regions of thick crust being delayed with respect to regions of thin crust. We have not corrected for these variations, because their magnitude depends on near-Moho velocity structure, which is not well known. We note, however, that such a correction would tend to *increase* the contrast of the NGA (that is, amplify it), since the NGA is strongest in coastal regions where the crust is thinnest.

#### 2.4. Calculation and interpolation of anomalies

Differential travel time anomalies were computed by subtracting the predicted differential travel time from the observed differential travel times. Finally, an overall mean was removed, so that the average differential travel time anomaly for each source group is zero.

The anomalies for each source group were interpolated onto a uniform two-dimensional grid using natural cubic splines. The interpolated data was contoured for visualization purposes; the contours emphasize the sharp gradients in travel time at the edges of the NGA (Fig. 5).

# 2.5. Tomographic inversion

S-wave data are inverted using RAYTRACE3D, a ray-based tomographic imaging code (Menke, 2005). The main purposes of the inversion are to accurately quantify the velocity contrast between the NGA and nearby craton, and to verify the NGA's overall shape, as directly deduced from the delay maps. The code represents velocities on a three-dimensional tetrahedral mesh and uses

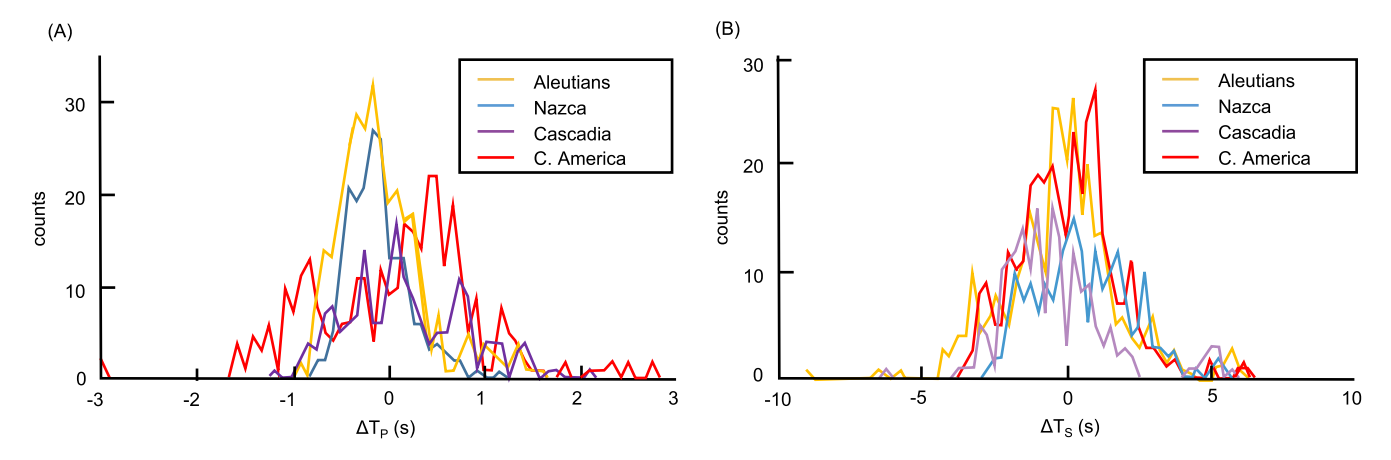


Fig. 4. Histograms of individual (one per seismic station) P and S differential travel times for each source group, with bin widths of 0.083 s for P-waves and 0.25 s for S-waves.

linear interpolation to infer velocities between nodes. It iteratively updates a laterally homogeneous starting model using linear least-squares to improve the fit to the observed differential travel time anomalies. Because of the limited azimuthal coverage, the mesh was intentionally made coarse, with a node spacing of 200 km horizontally and 100 in depth. The final iteration reduced the r.m.s. travel time residuals by 66.5% with respect to the starting model.

#### 3. Results

#### 3.1. Geospatial location and parallax

In the northeastern part of the study area, differential travel time anomalies are dominated by early arrivals from the North American craton, which is seismically fast owing to its being anomalously cold and depleted. The southwestern part is dominated by late arrivals from the NGA, which is seismically slow, because (as we will argue further) it is anomalously hot. All source groups consistently depict the late-to-early boundary as roughly linear and striking SE-NW. The Nazca and Aleutian source groups have nearly opposite back-azimuths of N163°E and N315°E, respectively. Furthermore, these back-azimuths are approximately parallel and anti-parallel to the strike of the boundary. Consequently, this boundary is particularly well-defined in the maps of delay times (Fig. 5), since most rays are entirely on one side of the boundary or the other. It is also very distinct in the tomographic inversion. We infer that it strikes about N142°E and approaches the Gulf Coast in westernmost Florida (near Pensacola).

For all source groups, late arrivals associated with the NGA extend from the western coast of the study region northward into the continental interior for at least 200 km (i.e. to at least 31°N). The pattern is wedge-shaped with tapering to the north, but varies significantly between source groups, presumably since each group provides a different two-dimensional projection of a three-dimensional object. About 400 km of parallax is observed between the NGA as illuminated by the Nazca and Aleutian source groups (which have nearly opposite back-azimuths) (Fig. 6).

#### 3.2. Amplitudes of differential travel times

Histograms of differential travel times anomalies indicate that all source groups have bell-shaped distributions of values (Fig. 4). Because the data are based on differential measurement, the mean of each distribution is arbitrary. The average width of the histograms (i.e. the maximum differential travel time anomaly with respect to the earliest value in the craton) is 3.2 s for P-waves and 7.2 s for S-waves. Some variation in the width of the distribution is observed. For example, the Central America source group has

a wider (by  $\sim$ 30%) histogram than the Cascadia source group, for both P-waves and S-waves. No extreme outliers are observed.

#### 3.3. Ratios of differential travel times

We used only the best travel time measurements (those having a waveform correlation coefficient >0.6) to estimate the ratio of P to S differential travel times anomalies (which we will later compare to laboratory measurements). The resulting best fit (Fig. 7), achieved by a least-squares fit that considers errors in both  $\Delta T_p$ and  $\Delta T_S$ , has a slope of 3.48  $\pm$  0.69 (95%). However, the mostpositive (i.e. latest) and most-negative (i.e. earliest) values fall systematically above the best-fit line, often by as much as 2 s. This difference is statistically significant, in the sense that the mean  $\Delta T_S$  of the right hand group (say with 1 s >  $\Delta T_p$  > 2 s) is unequal to the negative of the mean of the left hand group (say with  $-2 \text{ s} > \Delta T_p > -1 \text{ s}$ ) to >99% confidence. We fit a "kinked line" for comparison (Fig. 7). It confirms this behavior, with a slope of  $3.06 \pm 0.65$  (95%) to the left of the origin and a slope of  $4.35 \pm 0.71$  (95%) to the right of it. However, although the kinked line fits the data better than the straight line, it does so only to 75% confidence according to an F-test, probably because much of the data is for  $\Delta T_p \approx 0$ , a point that is well-fit by both models. Thus, we feel that the evidence for a difference in slope is fairly strong, but not overwhelmingly so.

### 3.4. Shear wave tomography

Both the low velocity NGA and the high velocity craton are easily identified in the tomographic inversion (Fig. 8) and their shapes and positions agree with those inferred from the delay maps. The position and strike of the NGA's eastern boundary is also confirmed. The NGA extends from about 250 to 400 km depth, but is most intense between 330-400 km depth, where it is 9.3% slower than the AK135 model at that same depth. The cratonic root is shallower, extending from the Moho to about 175 km depth and is most intense at 125 km depth, where it is 6.8% faster than the AK135 model at that same depth.

#### 4. Discussion

# 4.1. Depth extent of anomaly

Parallax in the pattern of delayed travel times caused by differences in seismic source direction can be used to estimate the depth at which the NGA is centered, as is illustrated in Fig. 6. The northern margin of the delayed region of the Nazca source group (with waves from the south) is displaced ~400 km northwestward

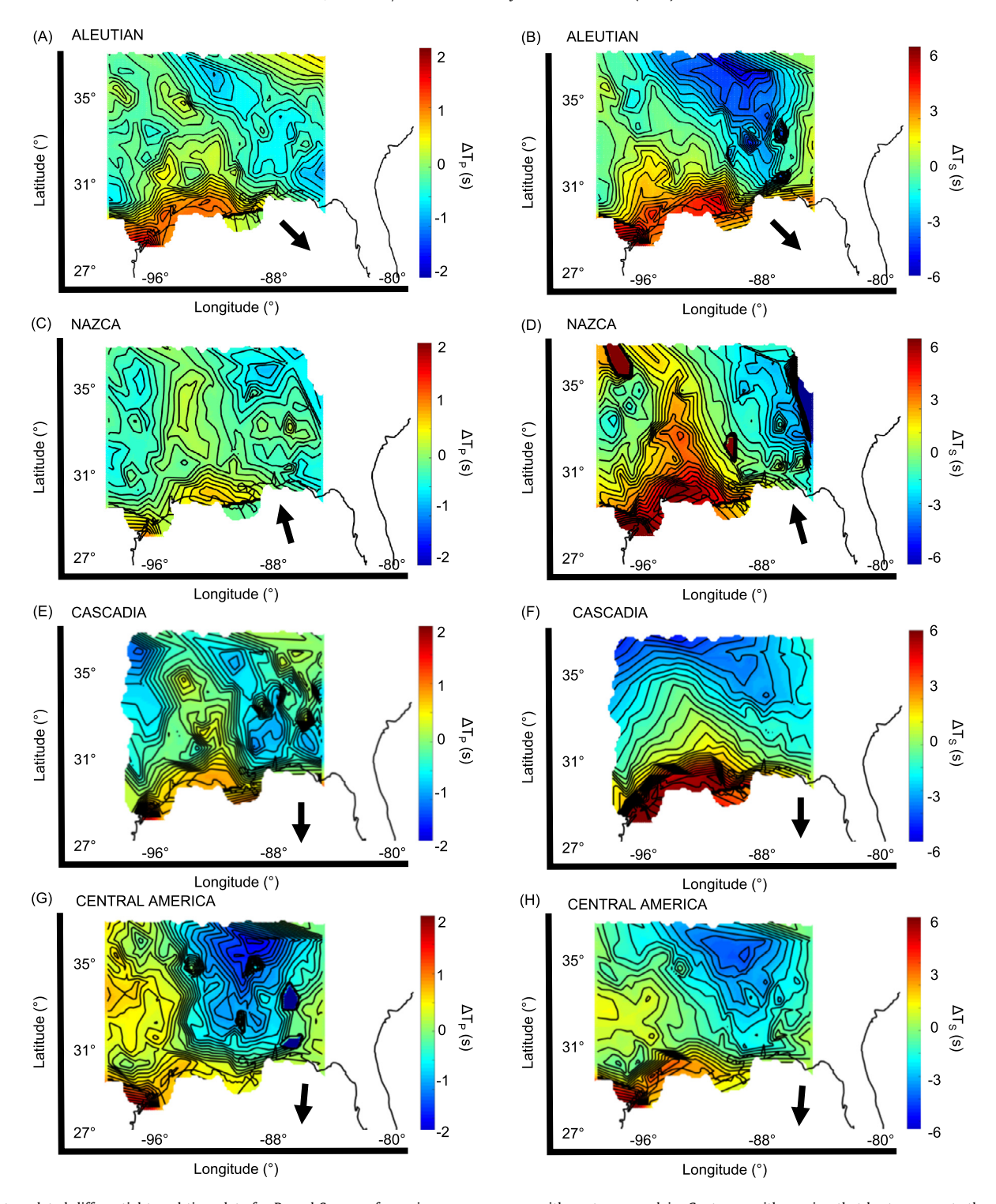


**Fig. 5.** Interpolated differential travel time data for P- and S-waves for a given source group, with contours overlain. Contours, with spacing that best represents the shape of the NGA, are shown at 0.1 s intervals for P-waves and 0.67 s intervals for S-waves. The black arrow in each subfigure represents the azimuthal direction to the teleseismic source group location.

with respect to that of the Aleutian group (with waves from the northwest).

The observed parallax is consistent with the 200-400 km depth range of the NGA as measured from the tomographic image (Fig. 8(c), (d)). This result confirms that the NGA is an asthenospheric anomaly with significant amplitude near the top of the transition zone. Our maximum depth is significantly deeper (by  $\sim$ 100) than Schmandt and Lin's (2014) continental-scale tomographic image and similar to Golos et al.'s (2018).

#### 4.2. Thermal character of anomaly

Differential delay times of up to 3.2 s for P-waves and 7.2 s for S-waves (after correction for sediment thickness) indicate the presence of an exceptionally strong anomaly. These values correspond to 7.6% and 9.5%, respectively, of reference travel times drawn from the AK135 Earth model. At 17%, the peak shear wave velocity anomaly, as determined by the tomography, is considerably higher, because the velocity heterogeneities are not uniformly

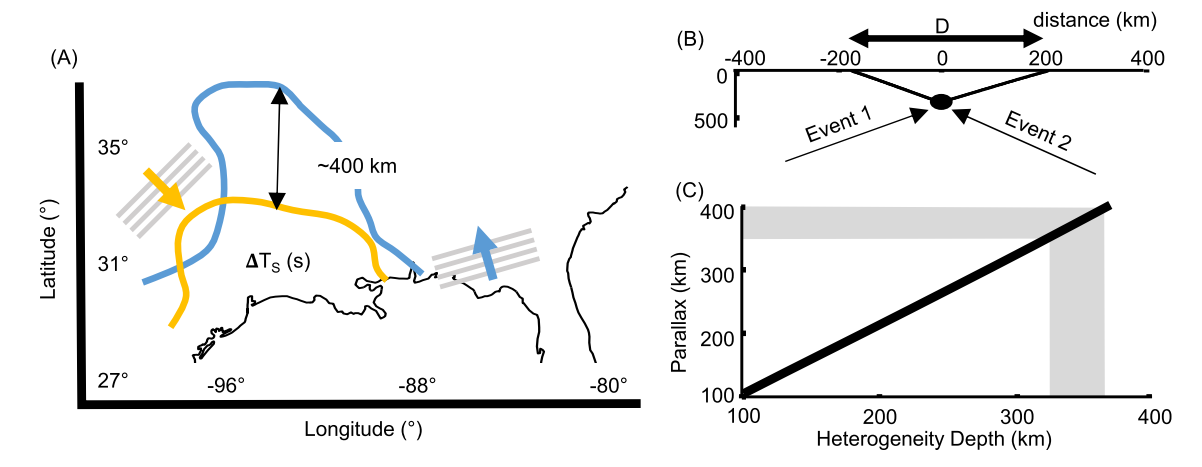
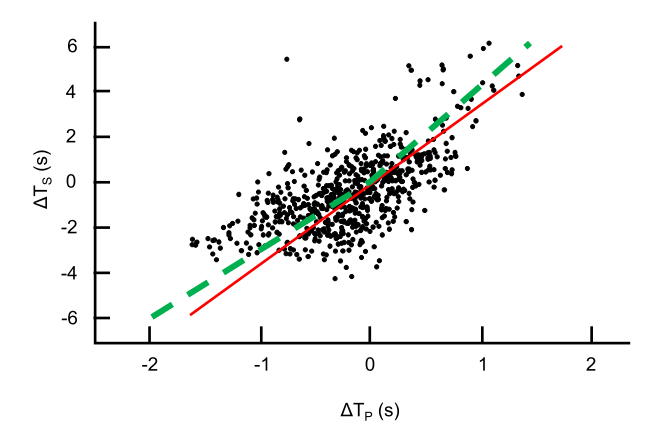


Fig. 6. (a) Rough outline of the NGA as shown by the S-wave trace of the Nazca (blue) and Aleutian (yellow) source groups, with their corresponding source azimuths shown in colored arrows. Comparison of the outlines shows ~400 km of parallax in the location of the anomaly in the North-South direction. (b) Depiction of parallax. Waves from events 1 and 2 pass through the same buried heterogeneity but separate to a parallax distance as they reach the Earth's surface. (c) Parallax distance as a function of heterogeneity depth. A parallax of 350-400 km corresponds to a heterogeneity depth of 330-360 km. Calculations are for rays from the Nazca and Aleutian source groups propagating through the AK135 Earth model.



**Fig. 7.** Plot of P versus S differential time delays for all 10 events, overlain by least squares best fit line (red) with a slope of 3.48. The "kinked" line with a shallower left-hand slope, created in consideration of the variations in distribution between negative and positive values, is shown in green.

distributed throughout the asthenosphere. However, this value is of questionable reliability, because it is very sensitive to the amount of regularization used to stabilize the inversion. The more meaningful estimate of 13% is obtained by noting that the average shear velocity anomaly in the central part of the NGA and craton are about -9% and 4%, respectively. These percentages are similar to those of the Northern Appalachian Anomaly (Menke et al., 2016), which is known to be an anomaly of high temperature and possible partial melt. It is also comparable to the average value for the Basin and Range province of the Western United States (relative to the North American craton). The maximum S-wave delay is larger than that observed for the Iceland hotspot (5.6 s relative to the periphery of the island) (Wolfe et al., 1997), and the East Pacific Rise ( $\sim$ 3 s, relative to the ridge flank 400 km away) (Toomey et al., 1998). This difference likely reflects the NGA extending to a greater depth than either the Iceland hotspot or the East Pacific Rise.

Rock physics experiments (Cammarano et al., 2003) predict the ratio of P to S velocity perturbations for a thermal anomaly to be  $\Delta V_s/\Delta V_p \sim 0.97$  (at a depth of 200 km and assuming a 1300 °C adiabat). The best fit line through NGA delay times (Fig. 7) has a slope of  $\mathrm{d}\Delta T_S/\mathrm{d}\Delta T_P = 3.48 \pm 0.69$  (95%). This slope, together with the estimates  $V_p = 8.47$  km/s and  $V_s = 4.63$  km/s drawn from the AK135 Earth model, imply  $\Delta V_s/\Delta V_p = 1.03 \pm 0.20$ . This value is equal, within the error, to Cammarano et al.'s (2003) pre-

diction of 0.97 for a thermal anomaly and significantly different than, to greater than 99% confidence, the expected ratio value for a chemical anomaly of 1/1.83. This result confirms that the NGA is a thermal anomaly.

The kink in the  $\Delta T_p$  vs.  $\Delta T_S$  plot (Fig. 7) hints that a second, weaker process is acting, in addition to temperature. One candidate is asthenospheric downwelling beneath the craton. Only the negative delays would be affected, since the craton is cold and fast. This vertical flow would lead to vertical alignment of the olivine a-axis (Ismail and Mainprice, 1998). If a rock with a random alignment of olivine axes begins with a P velocity of 8.34 m/s and an S velocity of 4.77 m/s, aligning the a-axis (fast axis) of the olivine vertically, and the other axes randomly, raises the P velocity to 9.20 m/s and the S velocity to 4.88 m/s. This corresponds to a 10% increase in P velocities and only a 2% increase in S-wave velocities. This significant increase in the speed of sub-vertically propagating Pwaves, with a much weaker increase in the speed of sub-vertically propagating S-waves, leads to a shallowing of the left-hand slope in Fig. 7. This hypothesis is supported by geodynamic modeling (Forte et al., 2010) that predicts strong downwelling in the craton near the NGA. This idea is also consistent with Wang and Becker's (2019, their Fig. 1b) continental-scale model of upper mantle anisotropy, which depicts the NGA as having strong (1.8 s) east-west oriented shear wave splitting, in contrast to the craton to the northeast, where splitting is much reduced (0.7 s).

# 4.3. Areal extent of anomaly

Differential delay times from all source groups were used to inform an interpretive plan-form diagram of the NGA (Fig. 8(b)), and cross-sectional views reveal the geometry at depth (Fig. 8(c), (d)) of the NGA. The northeastern boundary of the anomaly strikes N142°E, intersecting the edge of the continent at longitude 89°W, with decreasing intensity northwards. The central, intense part of the NGA extends to  $\sim$ 31N.

Our study, which lacks measurements within the Gulf of Mexico, does not directly constrain the southern boundary of the NGA. An indication of a southward extension can be found by comparing the histogram of delay times from varying back azimuths (Fig. 4). S-waves from the Central America source group (to the southwest), which traverse the asthenosphere beneath the Gulf, display a much wider (by  $\sim$ 2 s) distribution than waves traveling from the Cascadia source group (to the northeast), which mainly traverse the seismically fast material of the North American cra-

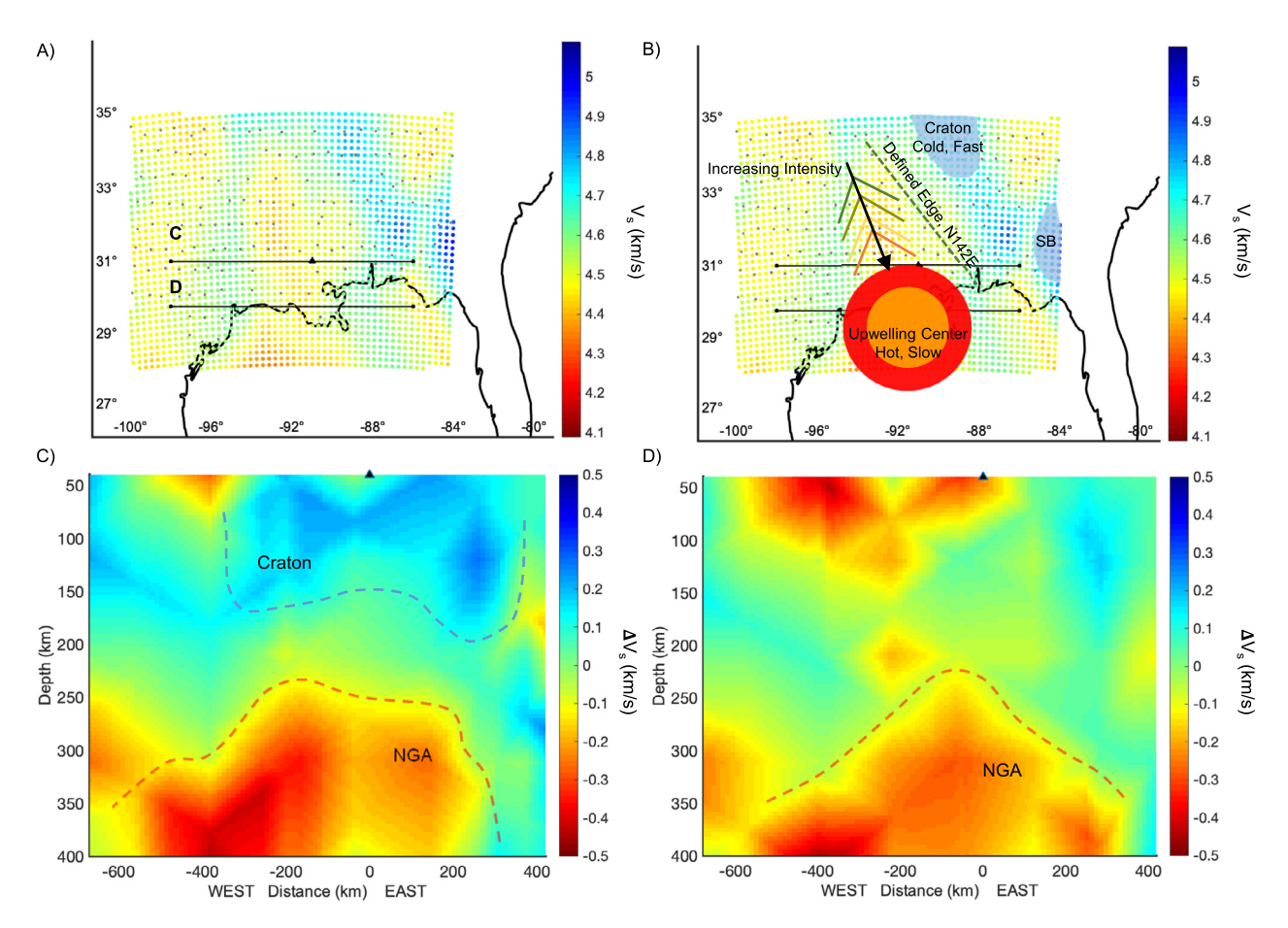


**Fig. 8.** (a) Shear wave velocity, as determined by the tomographic inversion. The locations of the cross sections in parts (c) and (d) are drawn with a black horizontal line, with the center of the array marked with a black triangle. (b) Schematic map of the study region, overlain on the results of the tomographic inversion. Red circle represents the observed main center of anomaly, with warmer colors representing increasing delay intensity. The newly defined margin of the anomaly is marked with a green dotted line. Cold regions, including the craton and Suwanee Block (SB, a pre-Gondwana accreted terrane) (Dallmeyer, 1988) are shown in blue. (c) Cross-sectional view of shear wave velocity through the center of the tomographic inversion, which clearly depicts the NGA (warm colors) and craton (cool colors). For ease of viewing, the NGA is outlined in red and the craton in blue. (d) Cross-sectional view of shear wave velocity through the proposed center of the NGA. These cross sections clearly depict the NGA as a low velocity zone with an elongate North-South geometry.

ton. These larger maximum delays of the Central America source group suggest that the NGA extends well offshore. Furthermore, the large delays extend to the Gulf Coast without any decrease in intensity, whereas all other edges of the NGA are gradational, a distinction that also suggests a southward extension. These inferences are consistent with the result of the tomographic inversion, which shows the anomaly extending offshore by at least 200 km, especially in the region south of the Louisiana-Texas border (longitude 94W). However, the resolution of this part of the inversion is poor, owing to the lack of anything but north-verging rays. Direct observation with ocean-bottom seismometers located within the Gulf itself would be necessary to resolve this issue definitively.

The NGA has been imaged in several recent investigations. The overall plan form of the NGA – a triangular wedge – is similar among all studies (including ours), but differs in significant detail. Schmandt and Lin (2014) image a clear NGA (at 200 km depth) and place its northernmost edge at 35°N,  $\sim\!400$  km north of our estimate, and its eastern intersection with the coast at 86°W, about  $\sim\!200$  km east of our estimate. Golos et al. (2018) image a clear NGA (at 390 km depth) with a plan form that is almost identical to Schmandt and Lin's (2014). Our study indicates that the NGA is much more concentrated along the Gulf Coast than has hitherto been realized, and has an area that is  $\sim\!50\%$  smaller than previous studies. The cross-sections produced by the tomographic inversion (Fig. 8(c), (d)) suggest an overall North-South elongate geometry at depth.

# 4.4. Thermal age of the NGA

The sharpness of a boundary between two materials of initiallydifferent temperature decreases with time, and can be used to infer an upper bound on the age of emplacement of the hotter material. We model the temperature evolution of the boundary between the NGA and craton, assuming a half-space Earth with zero-temperate top-surface boundary condition and a thermal diffusivity of  $8.5 \times 10^{-7}$  (Gibert and Seipold, 2003). The initial temperature of the NGA is modeled as uniform and 850 °C hotter than in the craton. The NGA is modeled as a triangular body, similar in size and shape to what is observed, and the boundary between it and the craton is vertical and initially 15-km thick. The time evolution is calculated analytically using the Green Function method (Carslaw and Jaeger, 1959). S-wave delays (at vertical incidence) are computed by converting temperature anomaly to shear velocity anomaly using Cammarano et al.'s (2003) relationship for the 1300 °C adiabat and integrating travel time increments along vertical straight-line rays. By  $\sim$ 200 Ma, the initially-sharp edge had become about as diffuse as is observed. Consequently, the possibility that the NGA represents a fossil feature dating from the opening of the Gulf of Mexico at ~180 Ma cannot be discounted, though the modeling does not preclude a younger age. However, the strong shear wave splitting at the NGA (Wang and Becker, 2019, their Fig. 9c) may be consistent with an old age, especially

if it represents a frozen-in lithospheric component dating from the time of rifting.

#### 5. Summary and conclusions

Teleseismic P- and S-wave travel time perturbations determined using the EarthScope Transportable Array (TA) data were used to identify and delineate the Northern Gulf Anomaly (NGA), a seismic anomaly beneath the northern coast of the Gulf of Mexico. After correction for the region's thick sediment cover, the data from this regional-scale passive-source study documents the strong intensity of the NGA. The large magnitude of delays (8% for P-waves and 10% for S-waves), together with their parallax with illumination direction, show the NGA to be a major feature extending throughout the asthenosphere. The observed ratio of P- and S-wave travel time anomalies imply that the anomaly is of thermal, not compositional, origin. This study produces a new estimate of the NGA's planform (Fig. 8(b)), improving upon previous studies (Schmandt and Lin, 2014; Golos et al., 2018) and indicating a triangular wedgeshaped anomaly, striking at N142E, likely centered within the Gulf of Mexico with a North-South elongate shape at depth. Terrestrial coverage by the TA is insufficient to locate the NGA's center; an ocean-bottom seismometer (OBS) array deployment within the Gulf will be required to image the anomaly in its entirety.

The presence of an anomaly as large and intense as the NGA in a seismically-quiet and passively-subsiding region is surprising, and raises questions regarding its origin and tectonic significance. Thermal modeling shows that the NGA could be a relic feature dating from the opening of the Gulf of Mexico at  $\sim$ 200 Ma, but the possibility of ongoing asthenospheric upwelling cannot be ruled out. The location of the NGA on the continental margin may indicate that it is a product of edge-driven convection, possibly analogous to other similar recently imaged thermal anomalies such as the Northern Appalachian Anomaly (Menke et al., 2016) and Central Appalachian Anomaly (Byrnes et al., 2019). These other continental-margin studies have recently been defined as areas of active upwelling (Biryol et al., 2016) associated with lithospheric foundering, displaying evidence of Tertiary volcanism and uplift. Although features associated with an opposite regime have been shown to exist in the Gulf region, the newfound existence of the NGA and its similarity to these upwelling-associated features suggests there may be evidence of upwelling (volcanism, rates of geodetic uplift, increased geotherm) in the Gulf region that either remains undiscovered, or currently misinterpreted. Future studies of shear wave splitting, which can distinguish regions of upwelling from regions of horizontal flow (Levin et al., 2017), as well as more detailed thermal modeling, may provide more insight into the origin of the NGA. This study reinforces the developing view of the asthenosphere beneath the passive continental margin of North America as hot and active, and as a potentially important source of lithospheric deformation.

#### **Declaration of competing interest**

The authors declare that they have no known competing financial interests or personal relationships that could have appeared to influence the work reported in this paper.

#### Acknowledgements

Z.K., who began this research while a Summer Intern at Lamont-Doherty Earth Observatory, thanks Program Director Dallas Abbott for her efforts in organizing and leading the Intern Program. This research was supported by the National Science Foundation under grants EAR 11-47742, OCE 13-59194 and EAR 11-47831.

#### References

- Adams, R.L., 2009. Basement tectonics and origin of the Sabine Uplift. Trans. Gulf Coast Assoc. Geol. Soc. 59, 3–19.
- Bird, D.E., Burke, K., Hall, S.A., Casey, J.F., 2005. Gulf of Mexico tectonic history: hotspot tracks, crustal boundaries, and early salt distribution. AAPG Bull. 89 (3), 311–328. https://doi.org/10.1306/10280404026.
- Biryol, C.B., Wagner, L.S., Fischer, K.M., Hawman, R.B., 2016. J. Geophys. Res., Solid Earth, 3393–3414. https://doi.org/10.1002/2015JB012698.
- Braunstein, J., McMichael, C.E., 1976. Door point: a buried volcano in southeast Louisiana. Trans. Gulf Coast Assoc. Geol. Soc. 26, 79–80.
- Byrnes, J.S., Bezada, M., Long, M.D., Benoit, M.H., 2019. Thin lithosphere beneath the central Appalachian mountains: constraints from seismic attenuation beneath the MAGIC array. Earth Planet. Sci. Lett. 519, 297–307. https://doi.org/10.1016/j. epsl.2019.04.045.
- Cammarano, F., Goes, S., Vacher, P., Giardini, D., 2003. Inferring upper-mantle temperatures from seismic velocities. Phys. Earth Planet. Inter. 138 (3–4), 197–222. https://doi.org/10.1016/S0031-9201(03)00156-0.
- Carslaw, H.S., Jaeger, J.C., 1959. The Conduction of Heat in Solids, 2nd edition. Oxford University Press, Oxford UK. ISBN 0198533683, 505 pp.
- Dallmeyer, R.D., 1988. Late Paleozoic tectonothermal evolution of the western Piedmont and eastern Blue Ridge, Georgia: controls on the chronology of terrane accretion and transport in the southern Appalachian orogeny. GSA Bull. 100, 702–713. https://doi.org/10.1130/0016-7606(1988)100<0702:LPTEOT>2.3.CO;2.
- Dokka, R.K., Sella, G.F., Dixon, T.H., 2006. Tectonic control of subsidence and south-ward displacement of southeast Louisiana with respect to stable North America. Geophys. Res. Lett. 33 (23), 1–5. https://doi.org/10.1029/2006GL027250.
- Dong, M.T., Menke, W.H., 2017. Seismic high attenuation region observed beneath southern New England from teleseismic body wave spectra: evidence for high asthenospheric temperature without melt. Geophys. Res. Lett. 44 (21), 10,958–10,969. https://doi.org/10.1002/2017GL074953.
- Ekstrom, G., 2014. Love and Rayleigh phase-velocity maps, 5-40 s, of the western and central USA from USArray data. Earth Planet. Sci. Lett. 402 (C), 42-49. https://doi.org/10.1016/j.epsl.2013.11.022.
- Ekstrom, G., 2017. Short-period surface-wave phase velocities across the conterminous United States. Phys. Earth Planet. Inter. 270, 168–175. https://doi.org/10.1016/j.pepi.2017.07.010.
- Fisk, H., Kolb, C., McFarlan, E., Wilbert, L., 1954. Sedimentary framework of the modern Mississippi Delta. J. Sediment. Res. 24 (2), 76–99. https://doi.org/10.1306/D4269661-2B26-11D7-8648000102C1865D.
- Forte, A., Moucha, R., Simmons, N., Grand, S., Mitrovica, J., 2010. Deep-mantle contributions to the surface dynamics of the North American continent. Tectonophysics 481, 3–15. https://doi.org/10.1016/j.tecto.2009.06.010.
- Gibert, B., Seipold, U., 2003. Thermal diffusivity of upper mantle rocks: influence of temperature, pressure, and the deformation fabric. J. Geophys. Res. 108, 2359. https://doi.org/10.1029/2002/B002108.
- Golos, E.M., Fang, H., Yao, H., Zhang, H., Burdick, S., Vernon, F., Schaeffer, A., Lebedev, S., van der Hilst, R.D., 2018. Shear wave tomography beneath the United States using a joint inversion of surface and body waves. J. Geophys. Res., Solid Earth 123 (6), 5169–5189. https://doi.org/10.1029/2017/B014894.
- Ismail, W.B., Mainprice, D., 1998. An olivine fabric database: an overview of upper mantle fabrics and seismic anisotropy. Tectonophysics 296 (1–2), 145–157. https://doi.org/10.1016/S0040-1951(98)00141-3.
- Kennett, B.L.N., Engdahl, E.R., Buland, R., 1995. Constraints on seismic velocities in the Earth from travel times. Geophys. J. Int. 122, 108–124. https://doi.org/10. 1111/j.1365-246X.1995.tb03540.x.
- King, S.D., Anderson, D.L., 1998. Edge-driven convection. Earth Planet. Sci. Lett. 160 (3–4), 289–296. https://doi.org/10.1016/S0012-821X(98)00089-2.
- Levin, M., Long, M.D., Skryzalin, P., Li, Y., López, I., 2017. Seismic evidence for a recently formed mantle upwelling beneath New England. Geology 46, 87–90. https://doi.org/10.1130/G39641.1.
- Menke, W., 2005. Case studies of seismic tomography and earthquake location in a regional context. In: Geophysical Monograph, vol. 157. American Geophysical Union, p. 7.
- Menke, W., Skryzalin, P., Levin, V., Harper, T., Darbyshire, F., Dong, T., 2016. The Northern Appalachian Anomaly: a modern asthenospheric upwelling. Geophys. Res. Lett. 43 (19), 10,173–10,179. https://doi.org/10.1002/2016GL070918.
- Menke, W., Lamoureux, J., Abbott, D., Hopper, E., Hutson, D., Marrero, A., 2018. Crustal heating and lithospheric alteration and erosion associated with asthenospheric upwelling beneath southern New England (USA). J. Geophys. Res., Solid Earth 123 (10), 8995–9008. https://doi.org/10.1029/2018/B015921.
- Mickus, K., Stern, R.J., Keller, G.R., Anthony, E.Y., 2009. Potential field evidence for a volcanic rifted margin along the Texas Gulf Coast. Geology 37 (5), 387–390. https://doi.org/10.1130/G25465A.1.
- Nettles, M., 2007. Analysis of the 10 February 2006: Gulf of Mexico earthquake from global and regional seismic data. Abstract OTC-19099-MS. In: Offshore Technology Conference.
- Pilger, J.R.H., 1981. The opening of the Gulf of Mexico: implications for the tectonic evolution of the northern Gulf Coast. Trans. Gulf Coast Assoc. Geol. Soc. 31, 377–381.

- Porter, R., Liu, Y., Holt, W.E., 2016. Lithospheric records of orogeny within the continental US. Geophys. Res. Lett. 43 (1), 144–153. https://doi.org/10.1002/ 2015G1066950
- Ryan, W.B.F., Carbotte, S.M., Coplan, J., O'Hara, S., Melkonian, A., Arko, R., Weissel, R.A., Ferrini, V., Goodwillie, A., Nitsche, F., Bonczkowski, J., Zemsky, R., 2009. Global multi-resolution topography (GMRT) synthesis data set. Geochem. Geophys. Geosyst. 10, Q03014. https://doi.org/10.1029/2008GC002332.
- Schmandt, B., Lin, F., 2014. P and S wave tomography of the mantle beneath the United States. Geophys. Res. Lett., 6342–6349. https://doi.org/10.1002/2014GL061231.
- Shen, W., Ritzwoller, M.H., 2016. J. Geophys. Res., Solid Earth, 4306–4342. https://doi.org/10.1002/2016JB012887.
- Stern, R.J., Anthony, E.Y., Ren, M., Lock, B.E., Norton, I., Kimura, J.I., Miyazaki, T., Hanyu, T., Chang, Q., Hirahara, Y., 2011. Southern Louisiana salt dome xenoliths: first glimpse of Jurassic (ca. 160 Ma) Gulf of Mexico crust. Geology 39 (4), 315–318. https://doi.org/10.1130/G31635.1.
- Toomey, D.R., Wilcock, W.S.D., Solomon, S.C., Hammond, W.C., Orcutt, J.A., 1998. Mantle seismic structure beneath the MELT region of the East Pacific rise from P

- and S wave tomography. Science 1224. https://doi.org/10.1126/science.280.5367.
- Tornqvist, T.E., Wallace, D.J., Storms, J.E.A., Wallinga, J., Van Dam, R.L., Blaauw, M., Derksen, M.S., Snijders, E.M.A., 2008. Mississippi Delta subsidence primarily caused by compaction of Holocene strata. Nat. Geosci. 1 (3), 173–176. https://doi.org/10.1038/ngeo129.
- Wang, W., Becker, T.W., 2019. Upper mantle seismic anisotropy as a constraint for mantle flow and continental dynamics of the North American plate. Earth Planet. Sci. Lett. 514, 143–155. https://doi.org/10.1016/j.epsl.2019.03.019.
- Wolfe, C.J., Bjarnason, I.T., Vandecar, J.C., Solomon, S.C., 1997. Seismic structure of the Iceland mantle plume. Nature 385 (6613), 245–247. https://doi.org/10.1038/385245a0
- Wolstencroft, M., Shen, Z., Tornqvist, T.E., Milne, G.A., Kulp, M., 2014. Understanding subsidence in the Mississippi Delta region due to sediment, ice, and ocean loading: insights from geophysical modeling. J. Geophys. Res., Solid Earth 119 (4), 3838–3856. https://doi.org/10.1002/2013jb010928.